Structure, Vol. 8, 1095–1103, October, 2000, ©2000 Elsevier Science Ltd. All rights reserved. PII S0969-2126(00)00508-6

3D Domain Swapping Modulates the Stability of Members of an Icosahedral Virus Group

Chunxu Qu,[1] Lars Liljas,[5] Natacha Opalka,[2,7] Christophe Brugidou,[2,8] Mark Yeager,[3] Roger N. Beachy,[2,4,9] Claude M. Fauquet,[2,9] John E. Johnson,[1,6] and Tianwei Lin[1,6]

[1]Department of Molecular Biology
[2]International Laboratory for Tropical Agricultural Biotechnology (ILTAB/IRD-DPSC)
[3]Department of Cell Biology
[4]Division of Plant Biology
The Scripps Research Institute
10550 North Torrey Pines Road
La Jolla, California 92037
[5]Department of Cell and Molecular Biology
Uppsala University
Box 596
751 24 Uppsala
Sweden

Summary

Background: Rice yellow mottle virus (RYMV) is a major pathogen that dramatically reduces rice production in many African countries. RYMV belongs to the genus sobemovirus, one group of plant viruses with icosahedral capsids and single-stranded, positive-sense RNA genomes.

Results: The structure of RYMV was determined and refined to 2.8 Å resolution by X-ray crystallography. The capsid contains 180 copies of the coat protein subunit arranged with $T = 3$ icosahedral symmetry. Each subunit adopts a jelly-roll β sandwich fold. The RYMV capsid structure is similar to those of other sobemoviruses. When compared with these viruses, however, the βA arm of the RYMV C subunit, which is a molecular switch that regulates quasi-equivalent subunit interactions, is swapped with the 2-fold-related βA arm to a similar, noncovalent bonding environment. This exchange of identical structural elements across a symmetry axis is categorized as 3D domain swapping and produces long-range interactions throughout the icosahedral surface lattice. Biochemical analysis supports the notion that 3D domain swapping increases the stability of RYMV.

Conclusions: The quasi-equivalent interactions between the RYMV proteins are regulated by the N-terminal ordered residues of the βA arm, which functions as a molecular switch. Comparative analysis suggests that this molecular switch can also modulate the stability of the viral capsids.

[6]To whom correspondence should be addressed (e-mail: jackj@scripps.edu and twlin@scripps.edu).
[7]Present address: The Rockefeller University, 1230 York Avenue, New York, New York 10021.
[8]Present address: Institut de Recherche pour le Developpement, Genetrop, B. P. 5045 34032 Montpellier Cedex 1, France.
[9]Present address: Donald Danforth Plant Science Center, Washington University, Campus Box 1229, One Brookings Drive, St. Louis, Missouri 63130.

Introduction

Rice yellow mottle virus (RYMV) is a pathogen that infects rice plants in western Africa. Its host range is limited to members of the family *Graminae*, principally *Eragrostidae* sp. and *Oryzae* sp. [1]. RYMV is readily transmissible by insect vectors, plant-to-plant contact, soil, and possibly irrigation water. The disease caused by RYMV has reached epidemic proportions, and has been known to reduce rice production by up to 100% [2]. RYMV caused rice cultivation to be abandoned for a number of years in several countries and it became a major constraint on rice production in the African continent [2].

RYMV is a member of the genus sobemovirus, a group of icosahedral plant viruses with southern bean mosaic virus (SBMV) as the type member [3]. RYMV contains a genome of single-stranded, positive-sense RNA of 4450 nucleotides [4]. A protein (VPg) is attached to the 5′ end of its genome and the RNA is not polyadenylated [4, 5]. The RYMV RNA contains four open reading frames, designated ORF1 to ORF4. ORF4 encodes a protein of 26 kDa, which forms the viral capsid.

RYMV particles are isometric and sediment uniformly at 109S during ultracentrifugation. The viral capsid is comprised of 180 copies of the coat protein arranged in a $T = 3$ quasi-equivalent surface lattice. The RYMV capsid is stabilized by divalent cations (Ca^{2+} and Mg^{2+}) [6]. The virion swells upon elevation of pH and removal of the cations by chelators [6]. A similar phenomenon is also observed in other plant viruses such as tomato bushy stunt virus (TBSV) [7, 8], southern cowpea mosaic virus (SCPMV; previously known as cowpea strain SBMV [3]) [9], and cowpea chlorotic mottle virus (CCMV) [10].

The crystal structures of two sobemoviruses, SCPMV and sesbania mosaic virus (SeMV), have been determined [9, 11]. Despite the wealth of structural knowledge on sobemoviruses, there is still great interest in structural studies of RYMV as it has different properties from other members in the family. The sequence identity between the RYMV and SCPMV coat proteins is about 22%; the sequence identity between SeMV and SCPMV coat protein is 62% [11]. Cryo-electron microscopy (cryoEM) and image reconstruction of SCPMV and RYMV to 25 Å resolution revealed that the two viruses were structurally similar under physiological conditions [12]. However, under swollen conditions SCPMV was so labile that few useful particles were obtained for the image reconstruction (data not shown). The swollen RYMV, on the other hand, was easily obtained and did not expand as much as anticipated for a sobemovirus. These findings suggested that the RYMV capsid was more stable than those of other sobemoviruses. This enhanced stability in the capsid could not be explained structurally by cryoEM and image reconstruction.

Here, we report the structure of RYMV determined by X-ray crystallography at 2.8 Å resolution. The RYMV structure reveals a major difference in the conformation of the regulator of the quasi-equivalent interactions, the βA arm (residues 30–53) of the C subunit. This arm in RYMV and other sobemoviruses makes comparable noncovalent interactions, however, its covalent association in RYMV has been swapped by 2-fold sym-

Key words: rice yellow mottle virus; Sobemovirus; virus assembly; virus structure; X-ray crystallography

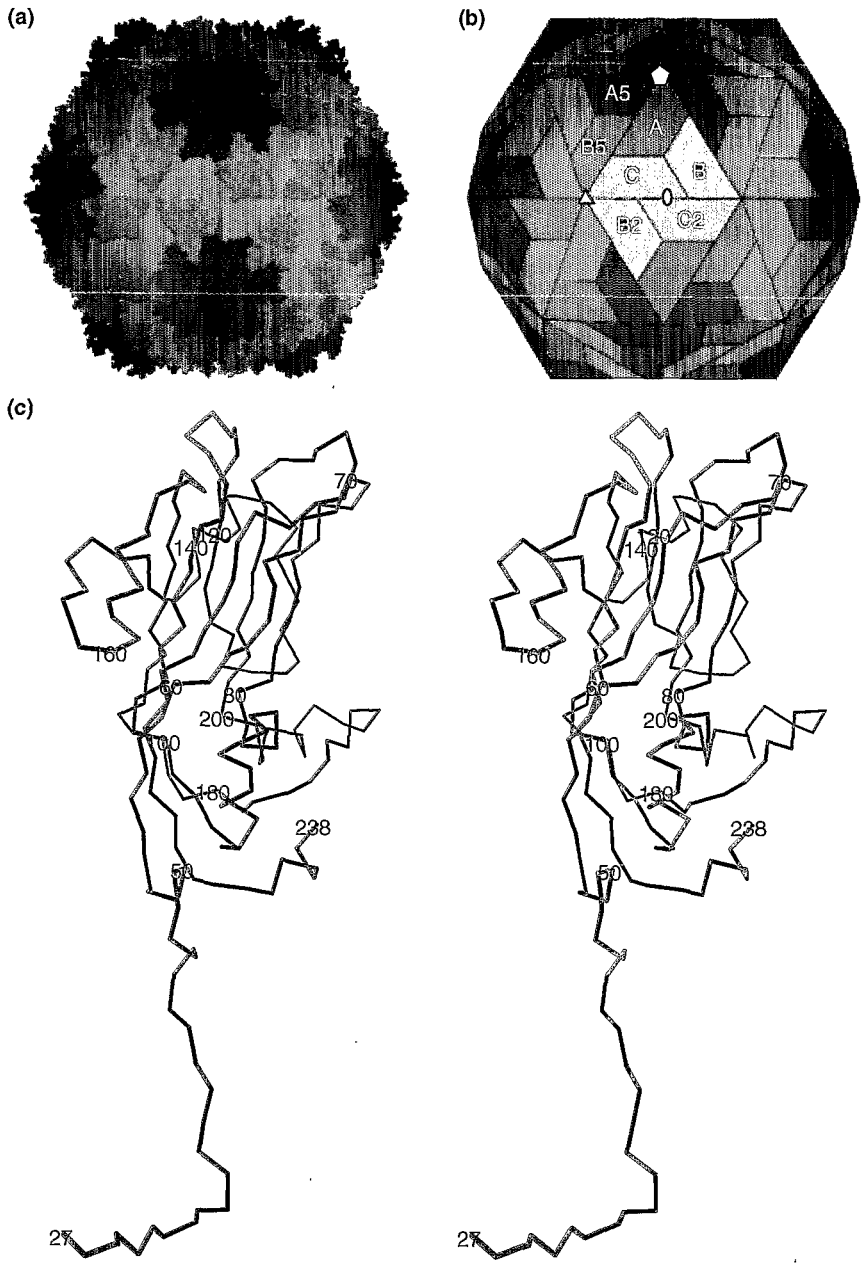

Figure 1. The RYMV Capsid Structure

The capsid comprises 180 copies of one single type of polypeptide arranged in $T = 3$ quasi-equivalent symmetry. The icosahedral asymmetric unit contains three subunits: A (in blue), B (in red), and C (in green). Each of the three subunits are of the same amino acid sequence, yet they occupy slightly different chemical environments.

(a) Space-filling model of the capsid. All atoms are shown as spheres of 1.8 Å in diameter. The CPK presentation was generated using the programs MOLSCRIPT [13] and Raster3D [14].

(b) Schematic representation of the capsid. Each trapezoid represents a β sandwich with jelly-roll topology of the same polypeptide. The letter designations are typical for $T = 3$ quasi-equivalent viruses. The symmetry axes of the icosahedron are also shown (in white): a pentagon for the 5-fold axis, a triangle for the 3-fold axis, and an oval for the 2-fold axis. Selected subunit types are labeled as A, B or C; the numbers following the letter indicate positions related by icosahedral symmetry to A, B, and C.

(c) The C subunit in stereoview. Residues 1–48 are not visible in the A and B subunits, but 22 of these residues (residues 27–48) can be modeled in the C subunit. These 22 additional ordered residues form the structural basis of a βA arm that serves as the switch regulating the quasi-equivalent symmetry (see text).

metry relative to other sobemoviruses. The enhanced stability of RYMV is attributed to this 3D domain swapping of the βA arms because it creates a network of long-range interactions not present in the other sobemovirus structures.

Results and Discussion

Structure of the Capsid

The RYMV capsid comprises 180 copies of the coat protein arranged with $T = 3$ quasi-equivalent symmetry. The overall shape of the virus particle is shown in Figure 1a as a space-filling model (generated with the programs MOLSCRIPT [13] and RASTER 3D [14]. The particle is nearly spherical, with small protrusions and depressions. The size of the particle is 250 Å across the 2-fold axis, 266 Å across the 3-fold axis and 292 Å across the 5-fold axis. Figure 1b shows a schematic representation of the capsid. The same gene product (that of ORF4, the capsid protein) occupies the A position (blue), which forms the pentamers, and the B and C positions (red and green), which cluster around the quasi-hexamers.

Structures of the Subunits

The subunits adopt a variation of the canonical eight-stranded jelly-roll β-sandwich fold found in most icosahedral viruses. Excluding the N-terminal 49 residues, which are disordered, 189 residues are modeled for the subunits in the A and B positions. These two subunits are virtually the same in structure and can be superimposed with a root mean square deviation (rmsd) of 0.4 Å for 189 Cα atoms. The fold of the capsid protein in the C position is nearly identical to those in positions A and B;

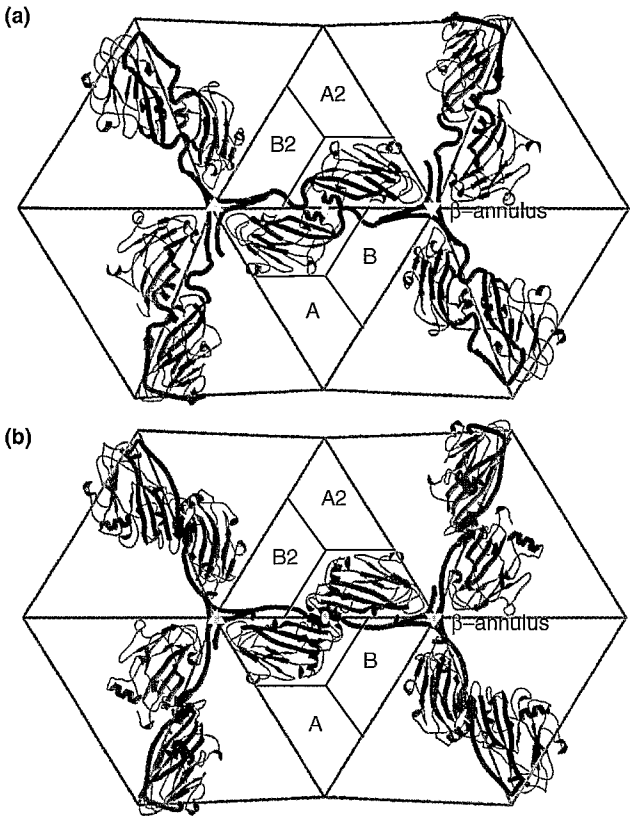

Figure 2. Interactions between C Subunits in the Sobemoviruses RYMV and SCPMV Viewed from the Interior of the Capsids

The C and 2-fold-related C2 subunits are colored in green and red, respectively. The positions of the A and B subunits in an icosahedral asymmetrical unit, as well as in the 2-fold-related asymmetrical unit, are marked. Cages showing the $T = 3$ quasi-equivalent surface lattices are drawn in yellow. The symmetry elements, triangles for 3-fold axes and ovals for 2-fold axes, are also in white. The β annuli are also shown.

(a) RYMV. The βA arm originating from the C subunit extends towards the B subunit, tucked between the B and C2 subunits, and forms a β annulus around the distal 3-fold axis. Subsequently, there is an interconnecting element in the capsid that knits the icosahedral asymmetric units together.

(b) SCPMV. The βA arm makes a "U turn" relative to the βB strand, forming the β annulus around the nearby 3-fold axis.

however, there are 23 additional residues (residues 27–49) ordered at the N terminus (Figure 1c). This extension of ordered residues near the N terminus (i.e., the βA arm) forms an additional β strand, βA, tucked between the subunits at B and C2 (2-fold-related C subunit), and a β annulus around the distal (relative to C) 3-fold axes (Figure 2).

A Molecular Switch

The construction of the $T = 3$ quasi-equivalent virus capsid of RYMV requires two types of subunit contacts from a single type of gene product. One type of interaction is exemplified by the A–A5 and C–B5 contacts, in which there is a bend between the two subunits, and it is termed as "bent contact" (Figure 3a). The other type of contact occurs between subunits adjacent to the icosahedral 2-fold axes (i.e., C–B2 and B–C2 contacts), and it is called the "flat contact" (Figure 3b). The bent and flat contacts are quasi-equivalent in the $T = 3$ surface lattice, but the difference in dihedral angles makes the quasi-6-fold axis a trimer of dimers in RYMV and other sobemoviruses (Figure 1b). A line of residue interactions is conserved in both bent and flat contacts and this is called the fulcrum. The switch between flat and bent contacts in the RYMV capsid is caused by the presence or absence of the βA arm (Figure 3). Wedged between the C and B2 subunits, the βA arm prevents the rotation about the fulcrum and forces the contact to be flat. Thus, the βA arm functions as a molecular switch that allows the $T = 3$ quasi-equivalent capsid to be constructed with a single type of building block. This kind of molecular switch has been observed in several $T = 3$ viruses [7, 9, 11]. The molecular switch observed in RYMV is different from those found in CCMV [10] and turnip yellow mosaic virus [15], where there are more ordered residues in the B and C subunits than in the A subunits and the quasi-hexamers are 6-fold symmetric. By contrast, the MS2 RNA phage forms $T = 3$ particles with a subunit that has an entirely different fold when compared with the β sandwich, and the mechanism for molecular switching is not apparent [16,17].

Comparison with Other Sobemoviruses: Quaternary and Tertiary Structures

A structure-based sequence alignment of the RYMV, SCPMV, and SeMV coat proteins is shown in Figure 4. As there is close structural similarity between SCPMV and SeMV, the following comparison is focused on the structures of RYMV and SCPMV. The quaternary organization of RYMV and SCPMV are the same. Although the sequence identity between RYMV and SCPMV is only 22%, the subunit structures are closely similar: the rmsd is 1.4 Å for the superposition of 176 Cα atoms of the corresponding subunits. The gaps in the sequence alignment (Figure 4) correspond to noticeable differences in structure, especially in the α helices of SCPMV. A six-residue deletion between βG and βH in the RYMV sequence reduced the helices αD and αE in SCPMV to one turn in RYMV. As the SCPMV helices αD and αE are on the surface and are involved in the interactions at quasi-3-fold axes, the removal of these two helices gives the appearance of a thinner shell around the quasi-3-fold axes in RYMV. This is in agreement with the structures obtained by cryoEM and image reconstruction. CryoEM showed that the exterior surface of SCPMV displayed deep valleys along the 2-fold axes and protrusions at the quasi-3-fold axes, whereas the surface of RYMV was comparatively smooth [12].

A second deletion in RYMV occurs between βF and βG (Figure 4), resulting in the removal of a disulfide bond that is observed in SCPMV. This difference is particularly noticeable at the 5-fold axis where the shorter sequence of RYMV enlarges the interior end of the axial channel from 12 Å in SCPMV to 16 Å in RYMV. The deletion reduces the thickness of the inner wall of the channel by 6 Å in RYMV. This is in agreement with cryoEM studies, where there is more electron density in the 5-fold axes of SCPMV [12].

A remarkable difference between RYMV and SCPMV is found near the N termini of the C subunits, where no major discrepancy is found in the sequence alignment (Figures 2 and 4). In both structures there are βA arms that serve as the molecular switches regulating the quasi-equivalent symmetry (see above). However, the βA arms of SCPMV and RYMV extend in opposite directions. The βA arm of SCPMV makes a "U turn" relative to the βB strand of the C subunit and tucks between the C and B2 subunits (Figure 2b). In this position βA creates a continuous ten-stranded β structure across the 2-fold symmetry axes with

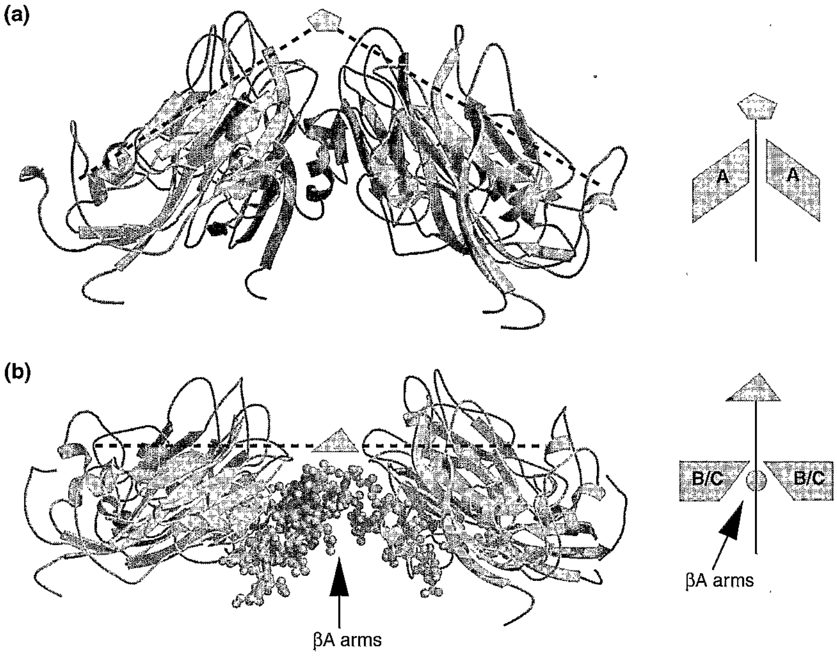

Figure 3. Subunit Dimer Contacts

(a) The bent contact, viewed perpendicular to the quasi 2-fold axis, looking from a 5-fold axis to a 3-fold axis. Without the βA arm, there is a dihedral angle of 144° between subunits at this joint. Subunits A and C are on one side; A5 and B5 are on the other side as shown in Figure 1b. The B and C subunits are blocked from view by the A subunits in this projection. (b) The flat contact, viewed perpendicular to an icosahedral 2-fold axis, along a line connecting adjacent 3-fold axes. The βA arm, shown in a CPK representation, forces the formation of the flat contact at this joint formed by subunits B and C on one side and 2-fold related B2 and C2 on the other, as shown in Figure 1b.

strands B, I, D, and G in the C subunits. In contrast, the βA arm of RYMV extends straight toward the B subunit and tucks between the B and C2 subunits (Figure 2a). Both of these arrangements of the βA arms are equally effective in making the flat contact, as the two 2-fold-related βA arms prevent bending in their noncovalent-bonding environments. However, the continuous β structure across the 2-fold axis in SCPMV is broken in RYMV. The interchange of chain connections in which a domain structure is conserved but is altered in position from proximal to distal relative to the remaining part of the covalently

```
                          *
RYMV:      1 ----- ----- -ARKG KKTNS NQGQQ GKRKS RRPRG RSAEP   29
SCPMV:     1 ATRLT KKQLA QAIQN TLPNP PRRKR RAKRR AAQVP KPTQA   40
SeMV:      3    LS IQQLA KAIAN TLETP PQPKA GRRRS AVQQL PPIQA   40
                 * * **βA-arm    *    **            *
RYMV:     30 QLQRA PVAQA SRISG TVPGP LSSNT WPLHS VEFLA DFKRS   69
SCPMV:    41 GVSMA PIAQG TMVKL RPPML RSSMD VTILS HCELS TELAV   80
SeMV:     41 GISMA PSAQG AMVRI RNPAV SSSRG AITVL HCELT AEIGV   80
             β-annulus              βA          βB
                           *            *    *            *
RYMV:     70 STSAD ATTYD CVPFN -LPRV WSLAR CYSMW KPTRW DVVYL  108
SCPMV:    81 TDTIV VTSEL VMPFT VGTWL RGVAQ NWSKY AWVAI RYTYL  120
SeMV:     81 TDSIV VSSEL VMPYT VGTWL RGVAD NWSKY SWLSV RYTYI  120
                    βC     αA'        αA         βD
             *        *  ***    ** * ** *        *   *  *
RYMV:    109 PEVSA TVAGS IEMCF LYDYA DTIPR YTGKM SRTAG FVTSS  148
SCPMV:   121 PSCPT TTSGA IHMGF QYDMA DTLPV SVNQL SNLKG YVTGP  160
SeMV:    121 PSCPS STAGS IHMGF QYDMA DTVPV SVNKL SNLRG YVSGQ  160
                          βE     ●   ●        αB        βF
             ** *   *                 *      *       *
RYMV:    149 VWYGA EGCHL LSGG- --SAR NAVVA SMDCS RVGWK R--VT  183
SCPMV:   161 VWEGQ SGLCF VNNTK CPDTS RAITI ALDTN EVSEK RYPFK  200
SeMV:    161 VWSGS AGLCF INNSR CSDTS TAIST TLDVS ELGKK WYPYK  200
                      αC                βG      αD        ●
                         *  *        ****                  *
RYMV:    184 SS--- -IPSS VDPNV VNTIL PARLA VRSSI K-PTV SDTPG  218
SCPMV:   201 TATDY ATAVG VNANI GNILV PARLV IAMEG GSSKT AVNTG  240
SeMV:    201 TSADY ATAVG VDVNI ATDLV PARLV IALLD GSSST AVAAG  240
                 αE                        βH
               *           *      *
RYMV:    219 KLYVI ASMVL RDPVD PTLNT                          238
SCPMV:   241 RLYAS YTIRL IEPIA AALNL                          260
SeMV:    241                TA SALNL                          260
                   βI           αF ●●
```

Figure 4. Amino Acid Sequence Alignment of the Capsid Proteins from RYMV, SCPMV, and SeMV

Residues in regular secondary structures that were defined using the program Molauto of MOLSCRIPT [13] are represented by bold letters. There are 44 conserved residues, which are indicated with asterices. The residues involved in calcium binding are indicated by spheres. The βA arms are boxed and residues of the β-annulus structure are marked with a gray bar. Residues proceeding the βA arm are not ordered in the C subunit; these residues, as well as the βA arm, are not visible in the A and B subunits.

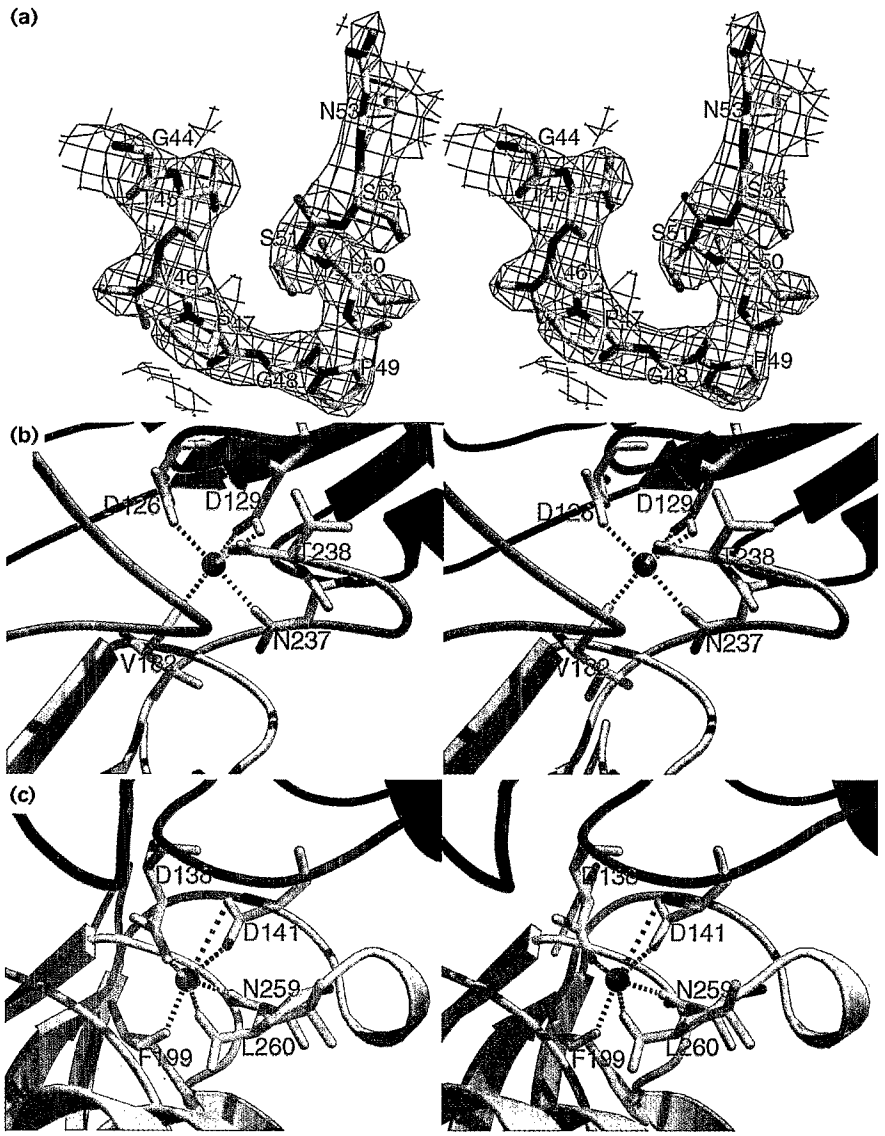

Figure 5. Stereoviews of the RYMV βA Arm and the Calcium Binding Sites in Two Sobemoviruses.

(a) The electron density of the peptide chain where the RYMV βA arm conformation differs from that of SCPMV. The electron density is shown as chickenwire and the polypeptide chain is in stick representation. The sequence Pro–Gly–Pro favors directional change of the peptide folding [23]. This figure was made using the program BOBSCRIPT [24]. The calcium binding site at the A–B subunit interface in (b) RYMV and (c) SCPMV. The A and B subunits are in blue and red, respectively. In (b), residues Asp126 and Asp129 in the A subunit and residues Val182, Asn237 and Thr238 in the B subunit are shown in ball-and-stick representation. In (c), residues Asp138 and Asp141 in the A subunit and residues Phe199, Asn259 and Leu260 are shown in ball-and-stick representation. Atoms of carbon, nitrogen and oxygen are in yellow, blue, and red, respectively. The calcium ions are drawn as 1Å spheres in magenta.

associated structure was first observed in the structure of diphtheria toxin [18]. This mechanism of subunit association was termed 3D domain swapping and adds stability to subunit associations; it is probably important in the evolution of oligomeric proteins [19]. Examples of 3D domain swapping were previously observed in the formation of dimeric structures [20] and two $T = 1$ viruses [21,22]. The exchange of βA arms in RYMV is the first example to show a role for 3D domain swapping in the formation of the capsid of a $T = 3$ virus.

The quaternary organization of the RYMV capsid does not seem to influence the direction in which the βA arms extend from the C subunits. However, the sequence of the junction at which the βA arm changes folding direction is Pro47–Gly48–Pro49 (Figure 5a). A sequence with proline residues is commonly associated with a change in chain direction and it was shown that such a sequence is usually found at the point of origin of a domain swap [23].

Comparison with Other Sobemoviruses: Subunit Contacts

The quaternary organization of the sobemoviral capsid is depicted schematically in Figure 1b. The unique interactions are A–B, A–C, B–C, A–A5, A–B5, C–B5, C–B2, C–C2. Table 1 shows the buried surfaces in the subunit contacts of the two viruses. It demonstrates that the interactions are generally more extensive in SCPMV than in RYMV. However, the relative buried surfaces between comparable subunits are similar, suggesting that the two viruses assemble via similar pathways.

A conserved feature of the interactions at the interface around the quasi-3-fold axis is the calcium binding site. Cal-

Table 1. Subunit Contacts

Interface	Total Buried Surface Area (Å²)		Percentage of Charged/ Polar Interactions	
	RYMV	SCPMV	RYMV	SCPMV
A–B	1578.3	1820.5	63.6	57.0
A–C	1522.8	1805.0	62.7	56.8
B–C	1521.5	1831.0	62.5	58.4
A–A5	1573.3	1745.4	52.6	56.5
A–B5	1100.6	1078.3	37.1	42.3
C–B5	1576.9	1974.4	50.7	56.2
BC–B2C2	4355.9	4843.2	44.2	46.4

Table 2. Hydrogen Bonds Observed at the β-Annulus Structures in RYMV and SCPMV

RYMV		SCPMV	
C C31	C C32	C C31	C C32
O Q30 Nη1 R41	N V36 O A34	O G41 N M52	N I47 O A45
O Q32 N A39	Nε2 Q38 Nη1 R33	N S43 O G50	O A48 N A45
Nη1 R33 Oε1 Q38	Oε1 Q38 Nη1 R33	O S43 N G50	N G50 O S43
Nη1 R33 Nε2 Q38	N A39 O Q32	N A45 O A48	O G50 N S43
O A34 N V36	Nη1 R41 O Q30	O A45 N I47	N M52 O G41

cium ions were found to be an important component of the SCPMV capsid [9], and analogous sites were found in the RYMV capsid as well (Figure 5b; generated using the program BOBSCRIPT [24]). Three calcium ions were identified on the basis of the electron-density map and are related by quasi-3-fold symmetry, as in the case of SCPMV (Figure 5c). They are located at the A–B, B–C and C–A subunit interfaces and have closely similar metal binding environments. For example, at the A–B interface there are three ligands from the A subunit and three from the B subunit. The ligands from the A subunit are carboxyl oxygens from the sidechains of Asp126 and Asp129, which are conserved among sobemoviruses (Figure 4). The ligands from the B subunit are two carbonyl oxygen atoms of the mainchain and the sidechain carboxyl oxygen from Asn237.

At the quasi-6-fold axes, 12 residues of the βA arms from 3-fold-related C subunits form an annular structure with β-strand-like hydrogen-bonding patterns (β annulus; Figure 2). Residue interactions of SCPMV and RYMV at the β annulus

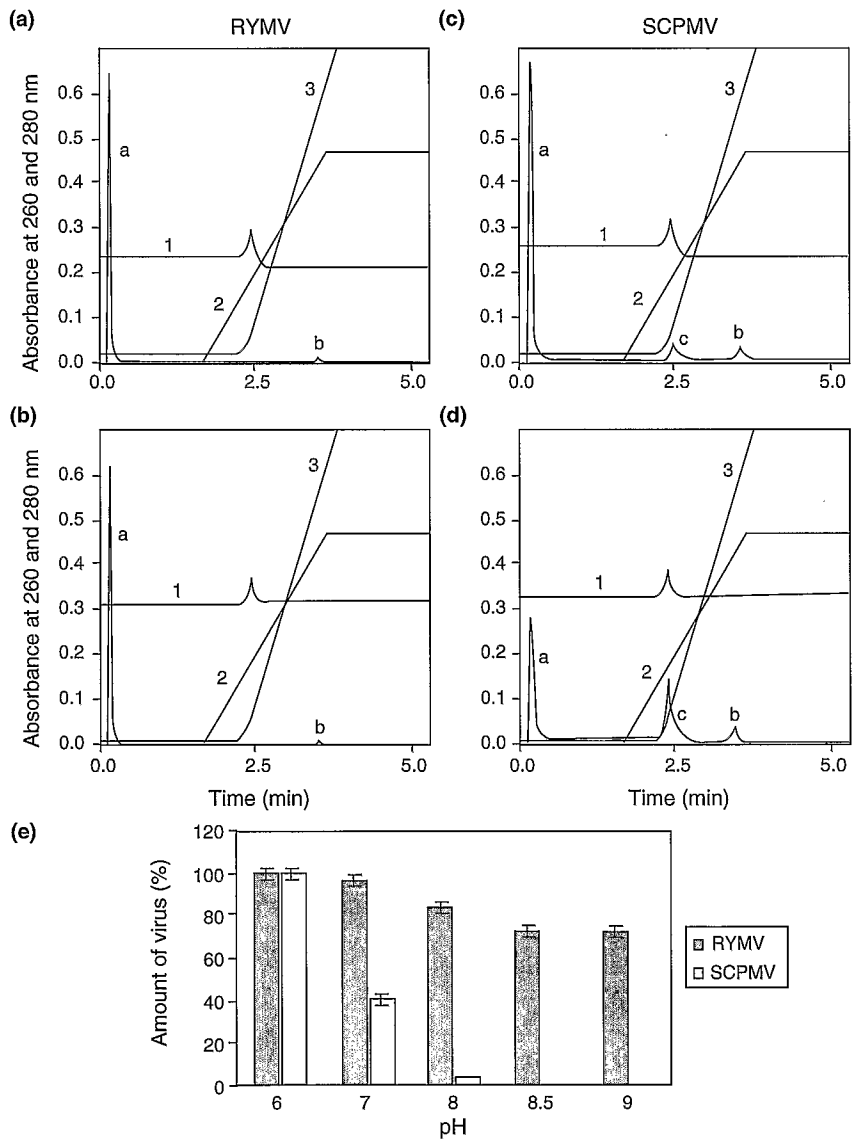

Figure 6. Comparison of the Capsid Stability of RYMV and SCPMV by Anion-Exchange Chromatography

Elution profiles for (a) RYMV at pH 6.0, (b) RYMV at pH 7.0, (c) SCPMV at pH 6.0, and (d) SCPMV at pH 7.0 are shown. Peak a corresponds to intact virus particles, Peak b corresponds to disassembled coat protein and peak c corresponds to nucleic acid. Line 1 indicates the pH, line 2 is for the salt gradient of NaCl changing from 0 to 2.55 M, and line 3 represents the conductivity. (e) Histogram of intact RYMV and SCPMV particles recovered from peak a at different values of pH.

are shown in Table 2. Although the two viruses have remarkably similar β annuli, the origins of the polypeptides are different as a result of the domain swapping. In SCPMV the βA arms from the C subunits nearest to the 3-fold axis contribute to the β annulus (Figure 2b), whereas in RYMV the βA arm from a distant C2 subunit (2-fold-related C subunit) forms the β-annular structure (Figure 2a). This is the result of the different directions in which the βA arms fold in the two viruses. The arrangement of βA arms in RYMV consequently produces long-range interactions, which knit the subunits into a web with polypeptide threads. The interlocking chain starts at the C2 subunit (residue 53) and is embedded between the C and B2 subunits (residues 53–40) as it extends toward the distal 3-fold axis, where it is fastened together with 3-fold related chains (residues 40–31) at the β annulus (Figure 2a). In contrast, the SCPMV βA arm interacts with the C subunit that it originates from. With the formation of the βA strand and β annulus around the 3-fold axis, the βA arms enforce the interactions of the hexamer; however, the interactions between hexamers are not as strong as those observed in the RYMV capsid (Figures 2b). A qualitative examination suggests that the swapped βA arms of RYMV make it globally more stable than SCPMV, an observation in agreement with the biochemical analysis of their stability (described later).

There are two other reported examples of 3D domain swaps in virus capsid proteins: in cricket paralysis virus (CrPV), a picorna-like insect virus [22], and *Galleria mellonella* densovirus (*Gm*DNV), an arthropod parvovirus [21]. The N terminus of the CrPV VP2 subunit, when compared with that of poliovirus, swaps with the 2-fold-related N terminus, maintaining comparable non-covalent interactions. The N terminus of the *Gm*DNV capsid protein, in comparison with that of a mammalian parvovirus, does the same thing. The swaps are comparable with those of the RYMV capsid proteins in the sense that the N-terminal regions make "U turns" relative to the direction of the chain following them sequentially in poliovirus and mammalian parvoviruses; however, the chain direction is continuous in the proteins of the corresponding viruses that infect insects. Only in RYMV, however, does the swap involve a molecular switch in a portion of the subunit. Picornaviruses and parvoviruses have no quasi-symmetry and require no switching.

Comparison with Other Sobemoviruses: Stability of the Capsids

A method was established to investigate the stability of RYMV particles by anion exchange in high performance liquid chromatography (C. B., O. N., M. Y., R. N. B., and C. M. F., unpublished data). It was shown that stable and intact virus particles were not retained by the resin and were eluted in the void volume. Unstable virus particles, on the other hand, did not maintain the integrity of the capsid under the pressure used in the chromatography and the component coat protein and nucleic-acid genome were eluted at different fractions in the salt gradient. This method was employed to compare the stabilities of RYMV and SCPMV.

As shown in Figures 6a and 6b, RYMV particles were eluted from the anion-exchange column operating at 1500 psi with a single peak at the void volume at pH 6 and pH 7, indicating that the particles were largely intact and the virus was stable. Decreased amounts of recovered virus (80% intact) were demonstrated by eluting the virus at pH 8. The amount of intact virus decreased to 70% at pH 8.5 and pH 9 (Figure 6e). SCPMV is largely stable at pH 6, showing a similar elution profile to that of RYMV (Figure 6c). However, elevation of the pH to 7 significantly reduced the amount of intact virus to 40% (Figure 6d). At pH 8, only 2.5% of the virus could be recovered. No viral particles could be detected at pH 9 (Figure 6e).

It is evident that RYMV is more stable than SCPMV under pressure and elevated pH. There is a high degree of similarity in the structure and interacting elements at the subunit interfaces of RYMV and SCPMV (Tables 1 and 2, Figure 5), and both contain aspartate residues as part of their calcium binding sites. Calcium sites at the subunit interface were suggested to be a pH-dependent regulatory element responsible for the viral polymorphism of CCMV [10]. In sobemoviruses, a similar argument can be used to explain the virus swelling. As pH rises, the deprotonated carboxy groups of aspartate residues of the calcium site at the interfaces repel one another. This repulsion between the subunits leads to the swelling and destabilization of the virus particle.

In the case of TBSV it has been proposed that the function of the βA arms in the C subunit and the β annuli is to determine the size of the virus particle during assembly [8]. If we assume that the members of the sobemovirus family adopt the same swelling pathway as TBSV, the β annular structure should be kept in the swollen state of RYMV and SCPMV, as observed in the 8 Å crystal structure of expanded TBSV [8]. Upon swelling, the interactions at the quasi-3-fold axis are disrupted, and subunits C and C2 slip away from each other. However, as shown in Figure 2a, the arrangement of the β annuli in RYMV limits the slip, providing additional force to maintain the virus integrity. With the β annuli kept in the structure, the maximum expansion allowed in RYMV might be determined by the ten-residue loop (residues from 44–53; Figure 5a). This is to say that the expanded state will straighten out this loop, but the particle cannot be expanded further without completely disrupting the capsid structure.

Biological Implications

Rice yellow mottle virus (RYMV) belongs to the *Sobemoviridae* family and 180 capsid proteins comprise the $T = 3$ capsid. Despite being generally similar to other sobemovirus structures, the regulator of quasi-equivalent interactions (the βA arm) is swapped to a symmetry-related and identical noncovalent bonding environment. Such a phenomenon has been observed in some other proteins in the formation of oligomers and has been termed "3D domain swapping". The 3D domain swapping introduces long-range interactions in the icosahedral surface lattice and enhances the stability of the RYMV capsid. Therefore the βA arm of sobemoviruses has a dual function: to regulate the quasi-equivalent interactions and to modulate the capsid stability.

Experimental Procedures

Virus Purification

The RYMV isolate used in this study was collected from rice fields in the Ivory Coast and was propagated under contained conditions in a susceptible rice variety IR8 (*Oryza sativa* L.) [25]. Two week old rice plants were infected by the virus using mechanical inoculation and grown in growth chambers. Six weeks after inoculation, the leaves were harvested and the virus was extracted (C. B., N. O., M. Y., R. N. B., and C. M. F., unpublished data). SCPMV was propagated in cowpea plants and purified according to the protocol described by Johnson et al. [26].

Crystallization, Structure Determination, and Refinement

RYMV was concentrated to 36 mg/ml by ultracentrifugation and suspension of the pellet in a small volume of 50 mM sodium acetate, pH 4.0, and 200 mM

lithium sulfate. The virus suspension was dialyzed exhaustively against the same solution. The crystallization was carried out by vapor diffusion and the reservoir solution was 50 mM sodium citrate, pH 3.0, 200 mM lithium sulfate, and 3.6% (w/v) PEG 8000.

A single crystal was used in the data collection by flash-cooling the crystal to −175°C under gaseous nitrogen. The cryo-protectant was made by adjusting the mother liquor to 25% (*R,R*)-2,3-butanediol. A data set was collected at the F1 station of the Cornell High Energy Synchrotron Sources with the Fuji Bas2000 imaging-plate system. The wavelength was 0.918 Å. The raw data were reduced and scaled using the HKL package [27]. The space group was determined as monoclinic $P2_1$ with cell dimensions of a = 283.5 Å, b = 401.8 Å, c = 284.0 Å, β = 89.4°. There are two virus particles in each unit cell. The completeness of the data was 48.7% to 2.8 Å with an R_{merge} of 7.2%. The orientation of the particle was determined by a self-rotation function algorithm [28, 29] and the position of the particle was calculated with an R factor search using X-PLOR [30], taking into account the particle packing in the crystal. RAVE [31] and CCP4 [32] program suites were used in the averaging, with the initial phasing model and mask derived from the SCPMV coordinates.

A polyalanine model without the βA arm of the C subunit of SCPMV[9] was initially built into the averaged density at 3.5 Å, and later proper side-chains were substituted using the program O [33]. The phases were calculated from the new model for new rounds of averaging. The βA arm of the C subunit was built on the basis of the gradual emergence of the corresponding electron density via multiple rounds of averaging. The model was refined with X-PLOR [30] using simulated-annealing methods [34], with data from 30.0 Å to 2.8 Å. In the final refinement, only the data with $F/\sigma(F) > 4.0$ were included and B factors were refined. An F_o–F_c difference map was calculated and 211 water molecules were modeled. The model was further refined by conjugated gradient minimization followed by B-factor refinement, and minor adjustments were made to the model. After two cycles of refinement and model building, water molecules with a B factor higher than 60 were rejected, and the averaged B factor for the remaining 191 water molecules was 36.7. The R factor is 22.7% for all the data between 50 and 2.8 Å. In the final model, no residue is in the disallowed region and 84% of the residues are in the most-favored region of the Ramachandran plot. The rmsd of the bond lengths is 0.008 Å and the rmsd of the bond angles is 1.4°.

Anion-Exchange Chromatography

Aliquots (50 μl) of RYMV and SCPMV (around 0.5 μg/μl) were used in the high performance liquid chromatography studies. A chromatographic system (PerSeptive Biosystems BIOCAD 700E, Cambridge, MA, USA) with an anion-exchange POROS column (10 μ particle size; column type: HQ/H, 4.6 mm D/100 mm L, CV= 1.7 ml) was used. The protocol employed in the chromatography will be published elsewhere (C. B., N. O., M. Y., R. N. B., and C. M. F., unpublished data). The elution buffer used was 15 mM of Bis-Tris Propane–Tris base (50/50, Sigma) at various values of pH (pH 6–9) at a flow rate of 6 ml/min under a pressure of 1250 psi. The maximum variation of three similar runs was 3%.

Acknowledgments

T. L. acknowledges very helpful discussions on crystallization with Enrico Stura. SCPMV was initially provided by David Hacker. Review of the manuscript by David Hacker before publication is also acknowledged. This work was supported by National Institutes of Health grant R01-GM 54076 (J. E. J.) and Burroughs Wellcome Fund on La Jolla Interface of Science.

Received: June 5, 2000
Revised: August 4, 2000
Accepted: August 7, 2000

References

1. Bakker, W. (1974). Characterisation and ecological aspects of rice yellow mottle virus in Kenya. Agric. Res. Rep. *829*, 152.
2. Abo, M.E. Sg, A.A., and Alegbejo, M.N. (1998). Rice yellow mottle virus (RYMV) in Africa: evolution, distribution, economic significance in sustainable rice production and development strategies. J. Sust. Agric. *11*, 85–111.
3. Hull, R., Fauquet, C.M., Gergerich, R.C., Lommel, S.A., and Thottapilly, G. (1999). Sobemovirus. In Virus Taxonomy. Seventh Report of the International Committee on Taxonomy of Viruses, M.H.V. van Regenmortel, et al., eds. (London, Academic Press), pp. 1014.
4. Ngon a Yassi, M., Ritzenthaler, C., Brugidou, C., Fauquet, C.M., and Beachy, R.N. (1994). Nucleotide sequence and genome characterization of rice yellow mottle virus RNA. J. Gen. Virol. *75*, 249–257.
5. Hull, R. (1988). The sobemovirus group. In The Plant Viruses: Polyhedral Virions with Monopartite RNA Genomes, R. Koening, ed. (New York: Plenum), pp. 113–146.
6. Hull, R. (1977). The stabilization of the particles of turnip rosette virus and of other members of the southern bean mosaic virus group. Virology *79*, 58–66.
7. Olson, A.J., Bricogne, G., and Harrison, S.C. (1983). Structure of tomato bushy stunt virus IV: the virus particle at 2.9 Å resolution. J. Mol. Biol. *171*, 61–93.
8. Robinson, I.K., and Harrison, S.C. (1982). Structure of the expanded state of TBSV. Nature *297*, 563–567.
9. Silva, A.M., and Rossmann, M.G. (1987). Refined structure of southern bean mosaic virus at 2.9 Å resolution. J. Mol. Biol. *197*, 69–87.
10. Speir, J.A., Munshi, S., Wang, G., Baker, T.S., and Johnson, J.E. (1995). Structures of native and swollen forms of cowpea chlorotic mottle virus determined by X-ray crystallography and cryo-electron microscopy. Structure *3*, 63–78.
11. Bhuvaneshwari, M., Subramanya, H.S., Gopinath, K., Savithri, H.S., Nayudu, M.V., and Murthy, M.R.N. (1995). Structure of *sesbania* mosaic virus at 3 Å resolution. Structure *3*, 1021–1030.
12. Opalka, N., et al., and Yeager, M. (2000). Structure of native and expanded sobemoviruses by electron cryo-microscopy and image reconstruction. J. Mol. Biol., in press.
13. Kraulis, P.J. (1991). MOLSCRIPT: a program to produce both detailed and schematic plots of protein structures. J. Appl. Crystallogr. *24*, 946–950.
14. Merritt, E.A., and Bacon, D.J. (1997). Raster3D Photorealistic Molecular Graphics. Methods Enzymol. *277*, 505–524.
15. Canady, M.A., Larson, S.B., Day, J., and McPherson, A. (1996). Crystal structure of turnip yellow mosaic virus. Nat. Struct. Biol. *3*, 771–781.
16. Valegård, K., Liljas, L., Firdborg, K., and Unge, T. (1990). The three-dimensional structure of the bacterial virus MS2. Nature *345*, 36–41.
17. Tars, K., Bundule, M., Fridborg, K., and Liljas, L. (1997). The crystal structure of bacteriophage GA and a comparison of bacteriophages belonging to the major groups of *Escherichia coli* leviviruses. J. Mol. Biol. *271*, 759–773.
18. Bennett, M.J., Choe, S., and Eisenberg, D. (1994). Domain swapping: entangling alliances between proteins. Proc. Natl. Acad. Sci. USA. *91*, 3127–3131.
19. Bennett, M.J., Schlunegger, M.P., and Eisenberg, D. (1995). 3D domain swapping: a mechanism for oligomer assembly. Protein Sci. *4*, 2455–2468.
20. Schlunegger, M.P., Bennett, M.J., and Eisenberg, D. (1997). Oligomer formation by 3D domain swapping: a model for protein assembly and misassembly. Adv. Protein. Chem. *50*, 61–123.
21. Simpson, A., Chipman, P.R., Baker, T.S., Tijssen, P., and Rossmann, M.G. (1998). The structure of an insect parvovirus (*Galleria mellonella* densovirus) at 3.7 Å resolution. Structure *6*, 1355–1367.
22. Tate, J.G., Liljas, L., Scotti, P., Christian, P., Lin, T., and Johnson, J.E. (1999). The crystal structure of cricket paralysis virus provides the first view of a new virus family. Nat. Struct. Biol. *6*, 765–774.
23. Bergdoll, M., Remy, M.-H., Cagnon, C., Masson, J.-M., and Dumas, P. (1997). Proline-dependent oligomerization with arm exchange. Structure *5*, 391–401.
24. Esnouf, R.M. (1997). An extensively modified version of MOLSCRIPT that includes greatly enhanced coloring capacities. J. Mol. Graph. *15*, 132–134.
25. Fauquet, C., and Thouvenel, J.C. (1977). Isolation of rice yellow mottle virus in Ivory Coast. Plant Disease Reporter *61*, 443–446.
26. Johnson, J.E., Rossmann, M.G., Smiley, I.E., and Wagner, M.A. (1979). Single crystal X-ray diffraction studies of southern bean mosaic virus. J. Ultrastruct. Res. *46*, 441–451.
27. Otwinowski, Z., and Minor, W. (1997). Processing of X-ray diffraction data collected in oscillation mode. Methods Enzymol. *276*, 307–326.
28. Tong, L., and Rossmann, M.G. (1990). The locked rotation function. Acta Crystallogr. A *46*, 783–792.
29. Tong, L., and Rossmann, M.G. (1997). Rotation function calculation with GLRF program. Methods Enzymol. *276*, 594–611.
30. Brünger, A.T. (1992). X-PLOR Version 3.1. A System for X-ray Crystallography and NMR (New Haven, CT: Yale University Press).

31. Kleywegt, G.J., and Jones, A.T. (1994). Halloween... mask and bones. In From First Map to Final Model, S. Bailey, R. Hubbard, and D. Waller, eds. (Daresbury, Warrington, UK: SERC Daresbury Laboratory), pp. 59–66.
32. Collaborative Computational Project Number 4. (1994). The CCP4 suite: programs for protein crystallography. Acta Crystallogr. D *50*, 760–763.
33. Jones, T.A., Zou, J.Y., Cowan, S.W., and Kjeldgaard, M. (1991). Improved methods for building protein models in electron density maps and the location of errors in these models. Acta Crystallogr. A *47*, 110–119.
34. Brünger, A.T., and Rice, L.M. (1997). Crystallographic refinement by simulated annealing: methods and applications. Methods Enzymol. *277*, 243–269.

Protein Data Bank Accession Codes

The coordinates have been deposited in the Protein Data Bank (accession code 1F2N).